SLAC-PUB-16488

Band gap opening in strongly compressed diamond observed by x-ray energy loss spectroscopy

E. J. Gamboa,[1] L. B. Fletcher,[1] H. J. Lee,[1] M.J. MacDonald,[1,2] U. Zastrau,[3] M. Gauthier,[1] D. O. Gericke,[4] J. Vorberger,[5] E. Granados,[1] J. B. Hastings,[1] and S. H. Glenzer[1]

[1]*SLAC National Accelerator Laboratory, 2575 Sand Hill Road, MS 72 Menlo Park, CA 94025 USA*

[2]*University of Michigan, 2455 Hayward St, Ann Arbor, MI 48109 USA*

[3]*High-Energy Density Science Group, European XFEL, Albert-Einstein-Ring 19, 22761 Hamburg, Germany*

[4]*Centre for Fusion, Space and Astrophysics, Department of Physics, University of Warwick, Coventry CV4 7AL, United Kingdom*

[5]*Institute of Radiation Physics, Helmholtz Zentrum Dresden-Rossendorf e.V., 01328 Dresden, Germany*

(Dated: January 25, 2016)

This material is based upon work supported by the U.S. Department of Energy, Office of Science, Office of Basic Energy Sciences, under Contract No. DE-AC02-76SF00515.

The extraordinary mechanical and optical properties of diamond are the basis of numerous technical applications [1] and make diamond anvil cells a premier device to explore the high-pressure behavior of materials [2]. However, at applied pressures above a few hundred GPa, optical probing through the anvils becomes difficult because of the pressure-induced changes of the transmission and the excitation of a strong optical emission [3]. Such features have been interpreted as the onset of a closure of the optical gap in diamond and can significantly impair spectroscopy of the material inside the cell [4]. In contrast, a comparable widening has been predicted for purely hydrostatic compressions, forming a basis for the presumed pressure stiffening of diamond and resilience to the eventual phase change to BC8 [5]. We here present the first experimental evidence of this effect at geo-planetary pressures, exceeding the highest ever reported hydrostatic compression of diamond by more than 200 GPa [6] and any other measurement of the band gap by more than 350 GPa. We here apply laser driven-ablation to create a dynamic, high pressure state in a thin, synthetic diamond foil together with frequency-resolved x-ray scattering as a probe. The frequency shift of the inelastically scattered x-rays encodes the optical properties and, thus, the behavior of the band gap in the sample [7]. Using the ultra-bright x-ray beam from the Linac Coherent Light Source (LCLS), we observe an increasing direct band gap in diamond up to a pressure of 370 GPa. This finding points to the enormous strains in the anvils and the impurities in natural Type Ia diamonds as the source of the observed closure of the optical window. Our results demonstrate that diamond remains an insulating solid to pressures approaching its limit strength [8]

Unlike most semiconductors, both the direct and indirect band gaps of diamond have been predicted to first increase with compression [9, 10] before decreasing and finally collapsing at extremely high pressures. Ab initio simulations have predicted a stable insulating phase under purely hydrostatic pressures of over 1 TPa [11, 12] and a band gap collapse at a combination of high uniaxial stresses >400 GPa and hydrostatic pressures of >100 GPa [13]. A red shift of the absorption edge and intense optical fluorescence has been observed at uniaxial pressures of over 300 GPa [4, 14]. However, it remains unknown whether this behavior is a consequence of the intrinsic closure of the diamond band gap at pressure,

is related to the impurities in natural diamond, or comes from deformation of the highly strained anvils.

In the context of planetary interiors [15], diamond is naturally compressed purely isotropically. The predicted opening of the band gap has been measured for hydrostatic pressures of <10 GPa by static compression experiments [16, 17]. Extending these measurements to extremely high pressures remains challenging experimentally, with the purely highest hydrostatic compression of diamond reported at a pressure of 140 GPa by Occelli et al [6]. Thus the band structure and electrical conductivity of diamond at planetary hydrostatic pressures remains largely unexplored in the laboratory.

Our present work represents the first observation of the nature of the direct band gap under large hydrostatic pressures, yielding quantitative measurements of the electronic structure of the insulating, cubic phase of diamond up to 370 GPa. Using dynamic compression from laser ablation, we can prepare a freestanding, nearly hydrostatically compressed diamond sample. We probe the band structure of the diamond by inelastic x-ray scattering from the LCLS free electron laser. The scattering spectra show a clear signature of collective plasmon excitations that characteristically shift to higher frequency losses with the increasing pressure. Combining these data with *ab initio* simulations reveals an opening of the band gap up to the highest observed pressures. Moreover, we can clearly rule out pressure-induced changes as a sources of the observed red shift of the optical absorption edge.

METHODOLOGY OF THE X-RAY PROBE

Observing the energy-loss of scattered x-rays is a well-established technique in dynamic compression experiments which can yield the material properties of warm dense matter or plasma states [18, 19]. In this regime, inelastic scattering comes primarily from free electrons that have been ionized or reside in the conduction band. Under certain conditions, the response of the electrons becomes collective and a plasmon is observed [7]. Such plasmons have also been observed in static compressions experiments with recent results from sodium at pressures up to 100 GPa [20].

A similar collective resonance can also be excited in insulators and semiconductors. Previous studies on non-metals have almost exclusively characterized thin membranes using

electron energy loss spectroscopy [21]. For dynamically compressed matter, where the high pressure and density state is maintained for only several nanoseconds, the record-brightness LCLS x-ray free electron laser provides a near ideal probe, permitting single-shot measurements of the inelastic x-ray scattering spectrum.

Valence electrons localized within chemical bonds in insulators can be collectively excited into an available conduction band. For diamond, the four sigma bonds then oscillate between bonding and anti-bonding states. The plasmon oscillation from the valence electrons couples to this additional vibrational mode, which is described by the Penn gap, or the average frequency separation between the valence and conduction bands. The resonance frequency for a scattered wave vector $\mathbf{k}$ may be modeled as

$$\omega(\mathbf{k}) = \sqrt{\omega_b^2 + \omega_{\mathrm{Penn}}^2} + \frac{\hbar^2}{m_e}\alpha\,\mathbf{k}^2\,. \tag{1}$$

Here, $\omega_b^2 = n_b e^2/m_e\epsilon_0$ is the plasma frequency associated with the valence electrons with density n_b and ω_{Penn} is the Penn gap frequency [22] between the valence and conduction bands. The additional quadratic dispersion term goes beyond the usual Drude model and is introduced following the behavior of the random phase approximation for free electrons. We have measured the empirical dispersion constant α to be 0.22 (See Supplementary Fig. S.I)

Taking $\omega_b = 31.1\,\mathrm{eV}$ from the valance electron density and $\omega_{\mathrm{Penn}} = 13.8\,\mathrm{eV}$ gives a plasmon loss of 34 eV for diamond under standard conditions [23, 24]. Under compression, the plasmon loss will shift to lower frequencies from both the densification and band gap opening. By independently constraining the density, we can experimentally determine the behavior of the band gap.

EXPERIMENTAL DETAILS

The experiment was performed at the Matter in Extreme Conditions (MEC) end station in the LCLS at the SLAC National Accelerator Laboratory. Figure 1(a) gives a schematic of the experimental setup. Thin foils of diamond, created by chemical vapor deposition, were heated and compressed by driving two counter-propagating pressure waves with intense optical lasers incident on each surface. Hydrodynamic simulations with the HELIOS code using the PROPACEOS equation of state tables [25] predict densities of up to $5\,\mathrm{g/cm^3}$ at

the collision of the two compression waves several nanoseconds after the start of the laser drive (see Fig. 1(b)).

The compressed samples were probed by 8 keV x-rays from the LCLS, focused to probe only the central, uniformly compressed region of the diamond. For each shot, we recorded inelastic spectra using a graphite crystal spectrometer as well as powder diffraction rings with an area detector in the forward direction [26]. The ultrafast x-ray pulse (80 fs) resulted in negligible time averaging from the motion of the compression waves. Examples for these two kinds of spectra are shown in Fig. 1(c) and (d). The angular shift of the Bragg peaks in the compressed samples directly provides the density; the spectral shift of the plasmon peak is sensitive to the changes in the electronic structure.

Figure 2 shows examples of inelastic scattering spectra measured at times near the coalescence of the ramp waves, thus sampling different density states. For comparison, we also show a control spectrum from undriven diamond. Applying Eq. (1), a larger density from the compression leads to an increase in the plasmon loss. These changes are reflected in the experimental spectra by a greater shift of the inelastic feature away from the elastic peak. We determine the plasmon frequency shift by fitting a theoretical spectrum to the data, with the total plasmon loss as a free parameter. The plasmon peak is shifted by up to 10 ± 1 eV from the position of the uncompressed diamond.

RESULTS AND DISCUSSION

We compare the measured plasmon shift to theoretical predictions in Fig. 3(a). Here, we first assumed a constant Penn energy. The increase of the electron density due to the compression is not sufficient to explain the data. The remaining increase of the plasmon energy must be attributed to an increase of the Penn gap. To improve our modeling, we also use Penn gaps that have been extracted from density functional theory (DFT) simulations (details in the Supplementary Materials). The DFT calculations predict an increase in the Penn gap under compression which, when inserted into Eq. 1, gives an excellent agreement with the measured plasmon shift.

The experimental data thus indicate an increase in the Penn gap from 13.8 eV at normal density to 20.5 eV at the maximum compression of 5.3 g/cc. Concomitant with the increasing Penn gap, the DFT simulations reveal a widening optical band gap. The calculated

pressure coefficient is approximately 5 meV/GPa for pressures up to 80GPa, 3meV/GPa up to 250Pa, and then 2meV/GPa to the highest simulated pressure of 800 GPa. These values are comparable to previous theoretical and experimental work at much lower pressures: 5 meV/GPa from the theoretical calculations by Fahy et al [10], 6 meV/GPa from the experiments of Onodera et al [17] to 2.3 GPa, and 6.9 meV/GPa at up to 7 GPa from Trojan et al [16]. The stiffening of the band structure at high pressures demonstrates that the material properties cannot be inferred from extrapolation from low pressure studies.

At elevated temperatures, thermal ionic motion can lead to a reduction in the band gap [27]. By observing the intensity of the elastically scattered peak, we measured the temperature of the diamond sample through the Debye Waller factor. The relative increase in the elastic peak yields a maximum temperature of 2800 K [28], which has a negligible impact on the DFT results (Supplementary Fig. S.II).

Under the large anisotropic stresses, typical of diamond anvil cells [3], the band gap of diamond has been predicted to collapse at pressures of 400 GPa [29]. Because our maximum inferred pressure is close to this value, it is important to consider non-hydrostatic effects that compress the lattice differently along each direction and may lead to a disagreement in the lattice constants, and thus density for different Bragg peaks. By measuring the shifts of the (111) and (220) diffraction peaks, we find the largest strain in our experiment results in a 0.03 Å anisotropy in the inferred lattice constants and an error of 5% in the density. Our DFT calculations show that this small amount of strain has only negligible effects on the band structure (Supplementary Fig. S.III). These small strains are in strong contrast to the 10% elongation of the lattice constant as predicted in highly strained diamond anvils [29].

In conclusion, we present the first measurements of the electronic structure of diamond at extreme pressures. Employing wavelength- and angular-resolved x-ray scattering simultaneously, we show that diamond remains an insulator to densities of at least 5.3 gcm^{-3} and pressures of 370 ± 25 GPa. Consistent with DFT simulations, we have observed the band gap of diamond to increase under compression. The stability of diamond under strong hydrostatic compression can have large implications for carbon-rich planets as a pressure-induced metallic phase has significantly different thermodynamic properties. Moreover, our results point to anisotropy and impurities as a source for the closure of the optical window in diamond anvil cells.

EXPERIMENTAL METHODS

The optical laser beams each delivered up to 4 J of light at 527 nm in a 4 ns long ramp pulse. The laser spots were smoothed with continuous phase plates giving a focal spot of 60 μm FWHM and a peak intensity of 70 TW/cm^2. The FEL beam was tuned to 8 keV and provided a typical pulse energy of 0.3 mJ of x-rays on target. The x-ray beam was focused to a spot size of 10 μm to probe the central region of the compressed diamond where conditions were most planar. Each shot destroyed the diamond sample and a fresh one replaced it.

Forward scattering spectra from the compressed diamond were recorded at a fixed angle of 25$\pm$0.26° using a highly oriented pyrolytic graphite crystal spectrometer. A Cornell-SLAC Pixel Array Detector observed Debye-Scherrer rings from x-ray diffraction over an angular range of 2θ = 17-55°, sufficient to observe the (111) and (220) diffraction peaks. We used the measured densities and temperatures to estimate the pressure from DFT equation of state calculations.

The diamond foils were prepared by chemical vapor deposition onto a silicon substrate seeded with a diamond powder. The samples were 3 x 3 mm at a thickness of 40 μm. The foil thickness was much greater than the relevant scale lengths of the x-ray interaction (the probe wavelength, plasma wavelength, and the electric field screening length) and the results are thus representative of bulk diamond.

The foil surfaces were analyzed using a profilometer showing an average grain size of 100 nm. The crystal grains show a typical preference to the orientation of the substrate planes[30]. The average density of the foils was measured using the profilometer and a microbalance as 3.45 g/cc. This is slightly less than the bulk density (3.51 g/cc) as measured by x-ray diffraction, which is explained by the formation of amorphous carbon at the boundaries of the crystal grains. This material contributes less than 2% of the signal at room temperature and is expected to assume the neighboring diamond phase at the elevated pressures. The main impurity was hydrogen adsorbed on the surfaces of the grains at a content of 0.1% by mass as estimated by electron energy loss spectroscopy.

---

[1] Nazare, M. H. & Neves (Eds.), A. J. *Properties, Growth and Applications of Diamond* (Institution of Engineering and Technology, 2000).

[2] Jayaraman, A. Diamond anvil cell and high-pressure physical investigations. *Rev. Mod. Phys.* **55**, 65–108 (1983). URL http://link.aps.org/doi/10.1103/RevModPhys.55.65.

[3] Ruoff, A. L., Luo, H. & Vohra, Y. K. The closing diamond anvil optical window in multi-megabar research. *J. Appl. Phys.* **69**, 6413–6416 (1991).

[4] Mao, H.-K. & Hemley, R. Optical transitions in diamond at ultrahigh pressures. *Nature* **351**, 721–724 (1991).

[5] Correa, A. A., Benedict, L. X., Young, D. A., Schwegler, E. & Bonev, S. A. First-principles multiphase equation of state of carbon under extreme conditions. *Phys. Rev. B* **78**, 024101 (2008).

[6] Occelli, F., Loubeyre, P. & LeToullec, R. Properties of diamond under hydrostatic pressures up to 140 gpa. *Nature Materials* **2**, 151–154 (2003).

[7] Glenzer, S. H. & Redmer, R. X-ray thomson scattering in high energy density plasmas. *Rev. Modern Phys.* **81**, 1625 (2009).

[8] Luo, X. *et al.* Compressive strength of diamond from first-principles calculation. *The Journal of Physical Chemistry C* **114**, 17851–17853 (2010).

[9] Goñi, A. R. & Syassen, K. Optical properties of semiconductors under pressure. *Semicondt. Semimet.* **54**, 247–425 (1998).

[10] Fahy, S., Chang, K. J., Louie, S. G. & Cohen, M. L. Pressure coefficients of band gaps of diamond. *Phys. Rev. B* **35**, 5856 (1987).

[11] Yin, M. T. & Cohen, M. L. Will diamond transform under megabar pressures? *Phys. Rev. Lett.* **50**, 2006–2009 (1983). URL http://link.aps.org/doi/10.1103/PhysRevLett.50.2006.

[12] Yin, M. T. Si-iii (bc-8) crystal phase of si and c: Structural properties, phase stabilities, and phase transitions. *Phys. Rev. B* **30**, 1773–1776 (1984). URL http://link.aps.org/doi/10.1103/PhysRevB.30.1773.

[13] Nielsen, O. H. Optical phonons and elasticity of diamond at megabar stresses. *Phys. Rev. B* **34**, 5808–5819 (1986). URL http://link.aps.org/doi/10.1103/PhysRevB.34.5808.

[14] Vohra, Y. K., Xia, H., Luo, H. & Ruoff, A. L. Optical properties of diamond at pressures of the center of earth. *Appl. Phys. Lett.* **57**, 1007–1009 (1990).

[15] Benedetti, L. R. *et al.* Dissociation of ch4 at high pressures and temperatures: diamond formation in giant planet interiors? *Science* **286**, 100–102 (1999).

[16] Trojan, I. A., Eremets, M. I., Korolik, M. Y., Struzhkin, V. V. & Utjuzh, A. N. Fundamental gap of diamond under hydrostatic pressure. *Jpn. J. Appl. Phys.* **32**, 282 (1993). URL `http://stacks.iop.org/1347-4065/32/i=S1/a=282`.

[17] Onodera, A. *et al.* Pressure dependence of the optical-absorption edge of diamond. *Phys. Rev. B* **44**, 12176–12179 (1991). URL `http://link.aps.org/doi/10.1103/PhysRevB.44.12176`.

[18] Glenzer, S. H. *et al.* Observations of plasmons in warm dense matter. *Phys. Rev. Lett.* **98**, 065002 (2007).

[19] Fletcher, L. *et al.* Ultrabright x-ray laser scattering for dynamic warm dense matter physics. *Nature Photonics* **9**, 274–279 (2015).

[20] Mao, H. K. *et al.* Electronic dynamics and plasmons of sodium under compression. *Proc. Natl. Acad. Sci. U.S.A.* **108**, 20434–20437 (2011).

[21] Egerton, R. F. Electron energy-loss spectroscopy in the tem. *Reports on Progress in Physics* **72**, 016502 (2009). URL `http://stacks.iop.org/0034-4885/72/i=1/a=016502`.

[22] Penn, D. R. Wave-number-dependent dielectric function of semiconductors. *Phys. Rev.* **128**, 2093 (1962).

[23] Ferrari, A. C. *et al.* Density, sp 3 fraction, and cross-sectional structure of amorphous carbon films determined by x-ray reflectivity and electron energy-loss spectroscopy. *Phys. Rev. B* **62**, 11089 (2000).

[24] Robertson, J. Diamond-like amorphous carbon. *Mater. Sci. Eng. R* **37**, 129–281 (2002).

[25] MacFarlane, J. J., Golovkin, I. E. & Woodruff, P. R. Helios-cr–a 1-d radiation-magnetohydrodynamics code with inline atomic kinetics modeling. *J. Quant. Spectrosc. Radiat. Transfer* **99**, 381–397 (2006).

[26] Gauthier, M. *et al.* New experimental platform to study high density laser-compressed matter. *Rev. Sci. Instrum.* (2014).

[27] Romero, N. A. & Mattson, W. D. Density-functional calculation of the shock hugoniot for diamond. *Phys. Rev. B* **76**, 214113 (2007).

[28] Gamboa, E. J. *et al.* Single-shot measurements of plasmons in compressed diamond with an x-ray lasera). *Physics of Plasmas* **22**, – (2015). URL `http://scitation.aip.org/content/aip/journal/pop/22/5/10.1063/1.4921407`.

[29] Surh, M. P., Louie, S. G. & Cohen, M. L. Band gaps of diamond under anisotropic stress. *Phys. Rev. B* **45**, 8239 (1992).

[30] Dawedeit, C. *et al.* Grain size dependent physical and chemical properties of thick cvd diamond films for high energy density physics experiments. *Diamond Relat. Mater.* **40**, 75 – 81 (2013).

ACKNOWLEDGEMENTS

This work was performed at the Matter at Extreme Conditions (MEC) instrument of LCLS, supported by the DOE Office of Science, Fusion Energy Science under contract No. SF00515. This work was supported by DOE Office of Science, Fusion Energy Science under FWP 100182. The target work was supported by a Laboratory Directed Research and Development grant. UZ was supported by the Peter Paul Ewald Fellowship of the VolkswagenStiftung.

AUTHOR CONTRIBUTIONS

EJG, DOG, JV and SHG co-wrote the manuscript. EJG, LBF, HJL, UZ, MJM, MG, EG, JBH, and SHG performed the experiment. EJG, LBF, MJM, UZ, MG, and SHG analyzed the spectra. JV and DOG performed calculations and simulations.

ADDITIONAL INFORMATION

Supplementary information is available in the online version of the paper. Correspondence and requests for materials should be addressed to EJG.

COMPETING FINANCIAL INTERESTS

The authors declare no competing financial interests.

FIGURES

Figure 1

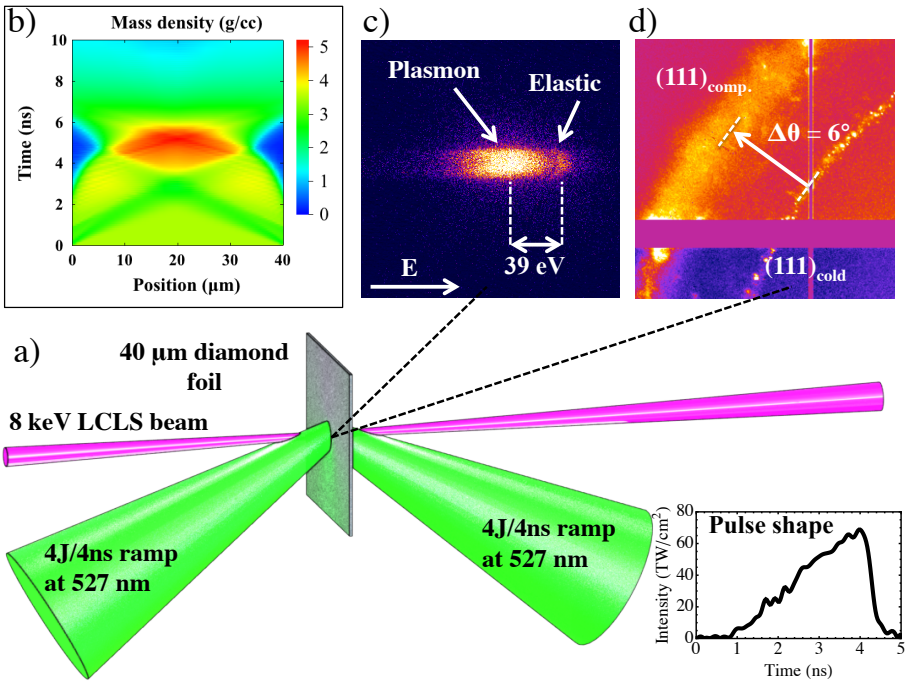

Figure 1. **Configuration for dynamic-compression experiment** (a) The diamond foils are compressed with a high-energy optical laser and probed with the high-photon flux x-ray beam from LCLS. The scattered x-rays are resolved in spectrum and angle. (b) Hydrodynamic simulations predict a density of $5\,\mathrm{gcm}^{-3}$ when the compression waves collide. c) Data for the inelastic scattering spectrum showing a distinct plasmon resonance. d) The Debye-Scherrer rings in the diffraction images are sensitive to the density of the sample.

Figure 2

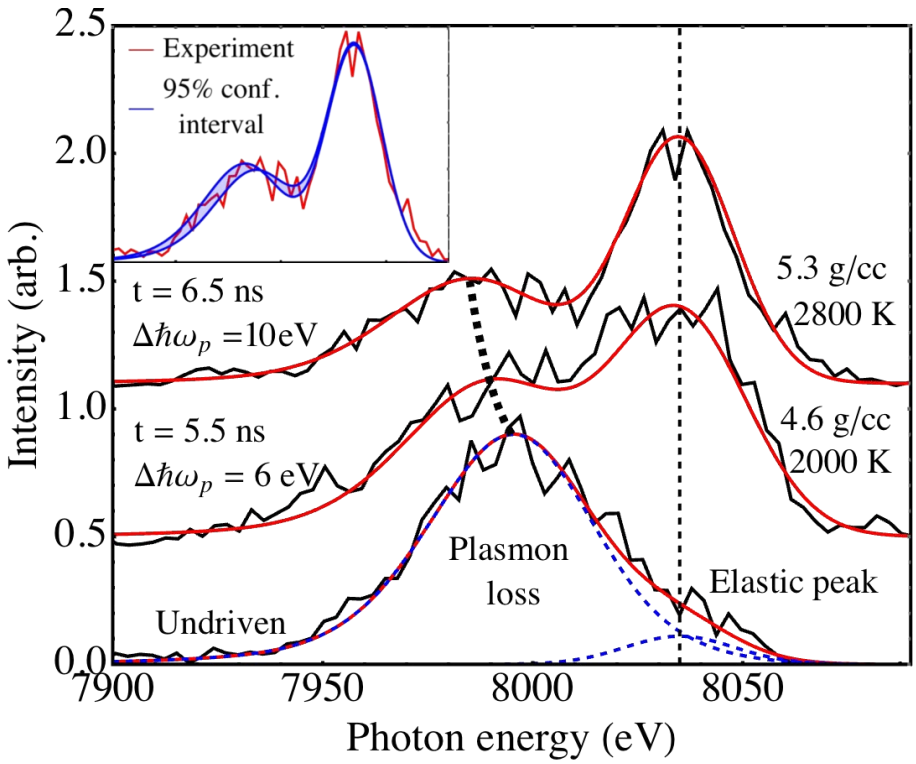

Figure 2. **Scattered spectra from compressed diamond.** The experimental data (black lines) preceding (5.5 ns) and at coalescence (6.5 ns) are compared to the synthetic spectra (red lines). The compressed shots show a downshift in the plasmon peak as compared to the undriven control sample. The blue dashed lines show the relative contributions to the scattering for the undriven spectrum, while the dashed line connects the centers of the plasmon peaks. Inset: the spectrum at 6.5 ns is compared to a 95% confidence interval for the fitted plasmon shift.

Figure 3

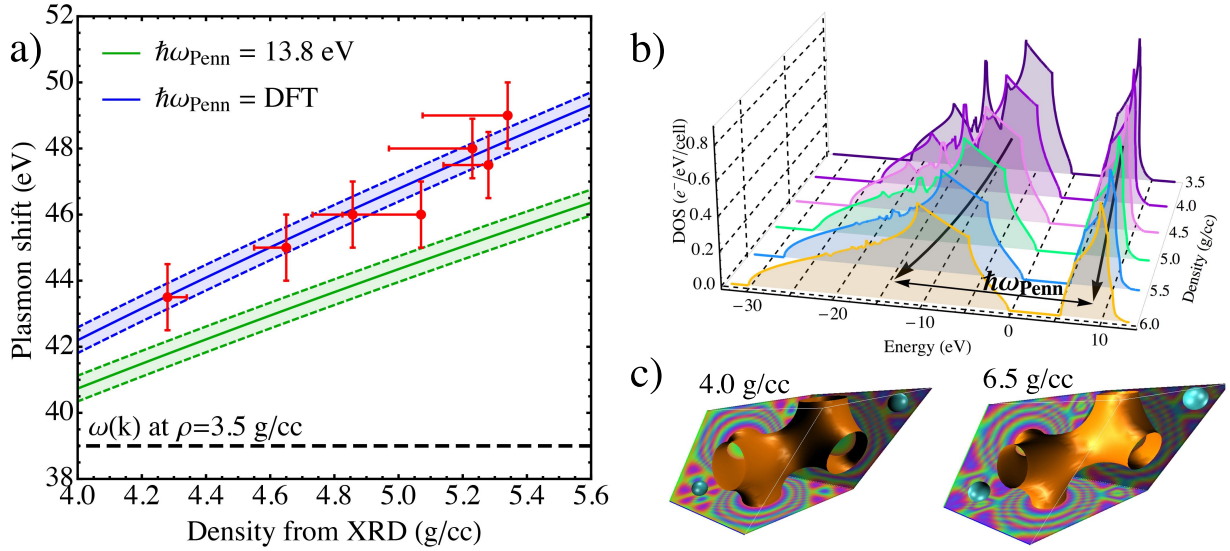

Figure 3. **Analysis of the inelastic scattering data.** (a) Measured plasmon shift versus density. The experimental data is compared to the two predictions using a constant band gap (green) and one inferred from DFT calculations of the density of states (blue). The density for the markers showing the experimental data is determined from the (111) diffraction peak with error bars inferred from the (220) peak. The dashed black line shows the plasmon shift of undriven diamond. (b) Density of states from the DFT calculations for different densities showing an opening of the band gap and modifications of the shape under compression. The arrows demonstrate the increase in the Penn gap with density c) Simulated isosurfaces of the valence electron density of diamond. Under compression the bound electrons move closer to the ions, widening the band gap and stiffening the material.

Supplemental Materials: Band gap opening in strongly compressed diamond observed by x-ray energy loss spectroscopy

E. J. Gamboa,[1] L. B. Fletcher,[1] H. J. Lee,[1] M.J. MacDonald,[1,2] U. Zastrau,[3] M. Gauthier,[1] D. O. Gericke,[4] J. Vorberger,[5] E. Granados,[1] J. B. Hastings,[1] and S. H. Glenzer[1]

[1]*SLAC National Accelerator Laboratory, 2575 Sand Hill Road, MS 72 Menlo Park, CA 94025 USA*

[2]*University of Michigan, 2455 Hayward St, Ann Arbor, MI 48109 USA*

[3]*High-Energy Density Science Group, European XFEL, Albert-Einstein-Ring 19, 22761 Hamburg, Germany*

[4]*Centre for Fusion, Space and Astrophysics, Department of Physics, University of Warwick, Coventry CV4 7AL, United Kingdom*

[5]*Institute of Radiation Physics, Helmholtz Zentrum Dresden-Rossendorf e.V., 01328 Dresden, Germany*

(Dated: January 25, 2016)

PLASMON DISPERSION

To obtain precise data for the plasmon dispersion, the diamond foils were probed with the seeded LCLS x-ray beam at 7.98 keV [1], which delivers on average 0.3 mJ of x-rays in a 40 fs, 0.01% bandwidth pulse. Forward scattering spectra were recorded over a range of angles from 5 to 30° using a von-Hàmos spectrometer with a high-resolution highly annealed pyrolytic graphite crystal and CCD detector. The low average dose and high transparency of the diamond to the x-rays leads to negligible heating by the FEL beam. The sample spectra in Figure S.I (a) were summed over approximately 700 shots each to accurately resolve the spectral shape.

We fit the quadratic dispersion of Eq. 1 to the measured plasmon shifts using the known value of the of zero-$\mathbf{k}$ plasmon shift [2]. From the fit, we infer a value of $\alpha = 0.22 \pm 0.016$ (see Fig. S.I (b)). Consistent with the findings of Batson and Silcox [3] in aluminum, the dispersion remains quadratic well past the critical wavevector, $\mathbf{k_c} \sim 1.6$ Å^{-1} for the transition to interband transitions of single electrons [4], indicating that the oscillation is primarily plasmonic in character. This interpretation is supported by the high-resolution experiments by Waidmann et al. [5], which showed the inelastic spectrum of diamond at $\mathbf{k} = 1.7$ Å^{-1} is dominated by the plasmon peak.

DFT CALCULATIONS

The DFT simulations of the electron band structure in diamond were performed with the code *abinit* [6]. The exchange correlation potential was taken in the Perdev-Burke-Ernzerhof type of the generalized gradient approximation [7]. We employed norm conserving pseudopotentials generated with the Troullier-Martins scheme via the FHI pseudopotential generator [8]. Four electrons per carbon atom are taken into account explicitly, the two $1s$ electrons in the core are frozen out. The energy cutoff was 35 Ha. The k-point sampling was performed using a Monkhorst-Pack grid of $32 \times 32 \times 32$ k-points [9]. This gives a convergence of pressure and energy of better than 0.1%. For the experimental lattice constant at normal conditions, we have tested exchange correlation potentials in the local density approximation (LDA) and the generalized gradient approximation (GGA) and obtained better pressure values for GGA (-6.5 GPa) than for LDA (-13.6 GPa). We also checked the electronic

density of state, band structure and elastic constants for ambient pressure and obtained reasonable agreement with known values.

For non-isentropic compression, there is a competition in the band gap between pressure-widening and closure from thermal ionic motion. For conditions along the shock Hugoniot, DFT calculations by Romero et al. predicted that the indirect band gap should begin to close at pressures above 160 GPa [10]. We assessed the effect of heating in these experiments by performing DFT calculations at elevated temperatures. Figure S.II displays the result of calculations of the band structure for 1.5 times compressed diamond at three different temperatures: 0 K, 5000 K, and 9000 K. The simulations indicate that the band gap has closed at the highest temperature, which suggests the transition to a conductive, liquid state similar to the observations of Bradley et al[11]. At 5000 K, the minimum band separation has decreased to nearly half of its T = 0 K value. However, the Penn gap has only reduced by about 1 eV from 20.2 to 19.2 eV which would lead to a decrease of less than half of an eV in the predicted plasmon position. Since this small shift is within the error bar from the fit to the angular dispersion and the observed temperature in these experiments are nearly a factor of two lower, we conclude that the temperature has a negligible effect on the Penn gap.

Figure S.III shows the effect of a strained lattice on the band structure for diamond at 5 g/cc. Similar to elevated temperatures, strains reduce the minimum separation between the bands. In the experiments, we infer a maximum strain in the lattice constant of 0.03 $\mathring{A}$. Our DFT calculations show that this small amount of strain would have almost no effect on the band structure and thus we can safely consider hydrostatic conditions for the DFT calculations in Fig. 3(a).

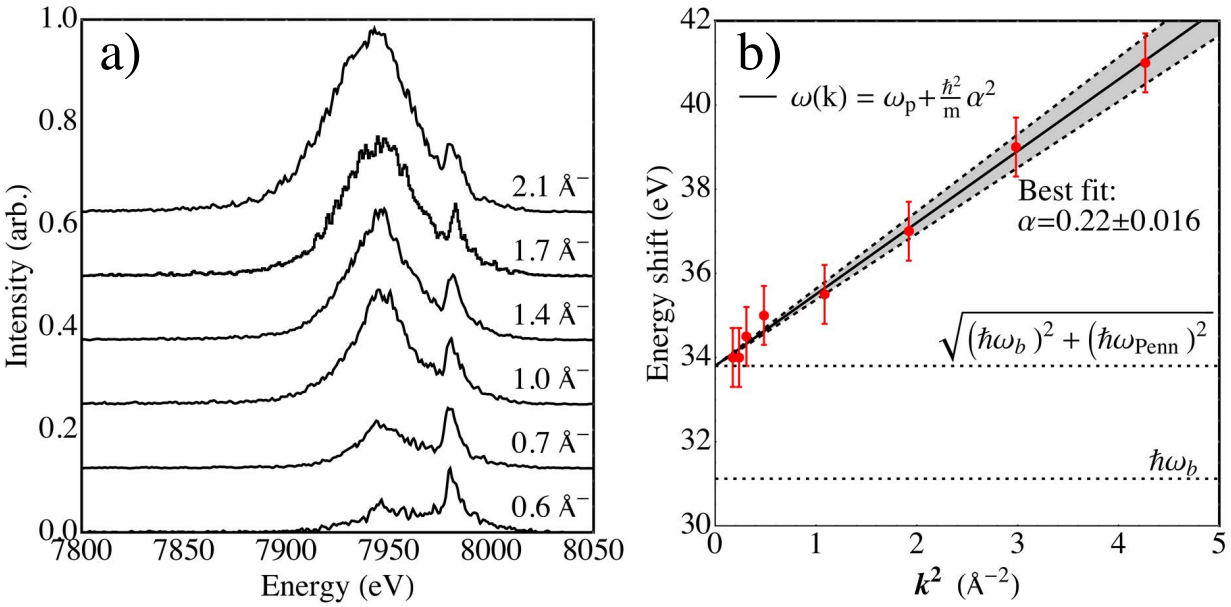

Figure S.I. **Empirically derived angular dispersion of the plasmon peak** Experimental forward scattering data (a) and the measured quadratic dispersion of the plasmon loss (b). The shaded area between the dashed lines establishes a 95% confidence interval to the best fit value for α.

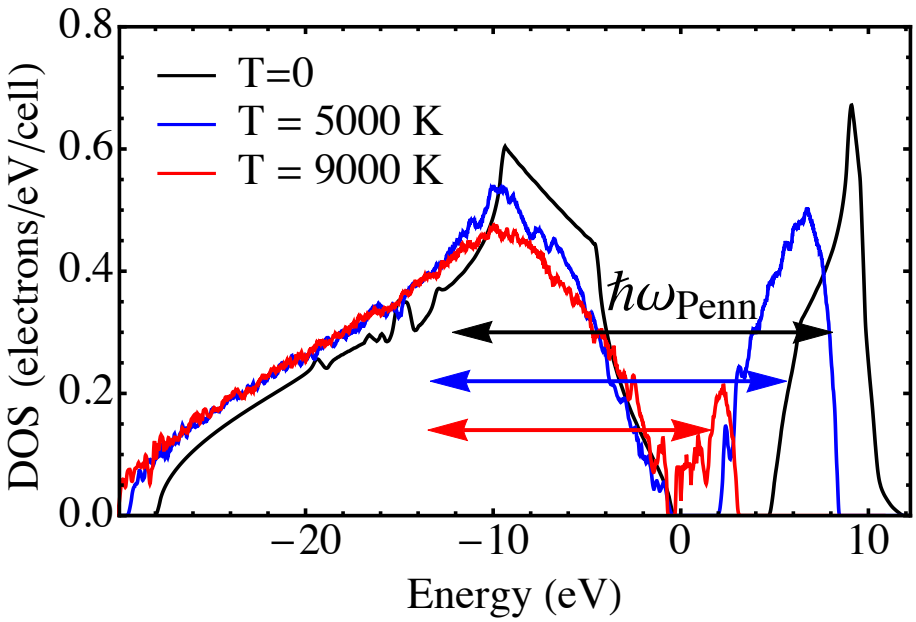

Figure S.II. **DFT simulations of band structure at finite temperature for diamond at 5.3 g/cc**

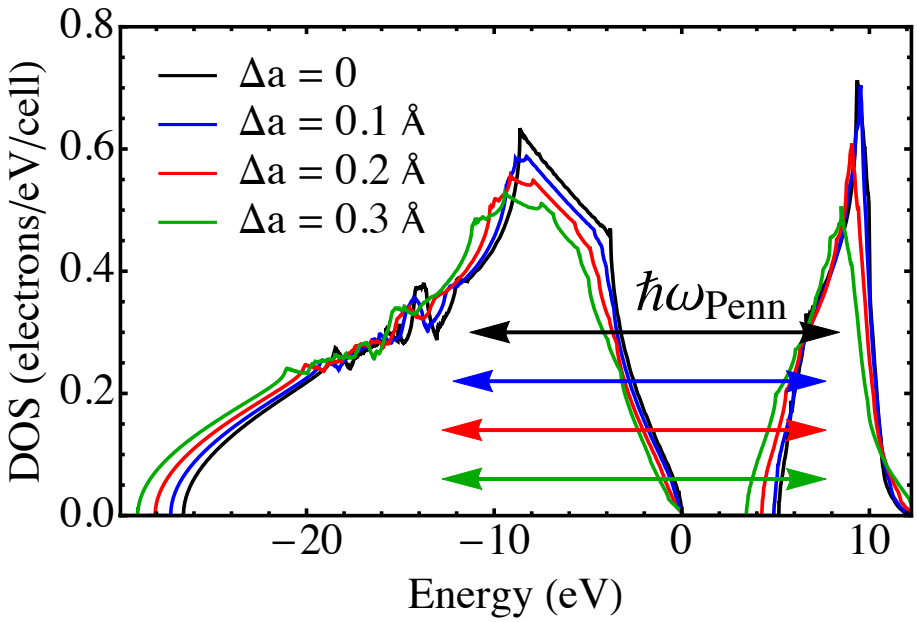

Figure S.III. **DFT simulations of band structure for strained diamond at 5.0 g/cc**

[1] Amann, J. *et al.* Demonstration of self-seeding in a hard-x-ray free-electron laser. *Nature Photonics* **6**, 693–698 (2012).

[2] Robertson, J. Diamond-like amorphous carbon. *Mater. Sci. Eng. R* **37**, 129–281 (2002).

[3] Batson, P. & Silcox, J. Experimental energy-loss function, im [-1 ε (q, ω)], for aluminum. *Phys. Rev. B* **27**, 5224 (1983).

[4] Schülke, W., Bonse, U., Nagasawa, H., Kaprolat, A. & Berthold, A. Interband transitions and core excitation in highly oriented pyrolytic graphite studied by inelastic synchrotron x-ray scattering: Band-structure information. *Phys. Rev. B* **38**, 2112–2123 (1988). URL `http://link.aps.org/doi/10.1103/PhysRevB.38.2112`.

[5] Waidmann, S. *et al.* Local-field effects and anisotropic plasmon dispersion in diamond. *Phys. Rev. B* **61**, 10149–10153 (2000). URL `http://link.aps.org/doi/10.1103/PhysRevB.61.10149`.

[6] Gonze, X. *et al.* Abinit: First-principles approach to material and nanosystem properties. *Comput. Phys. Commun.* **180**, 2582–2615 (2009).

[7] Perdew, J. P., Burke, K. & Ernzerhof, M. Generalized gradient approximation made simple. *Phys. Rev. Lett.* **77**, 3865 (1996).

[8] Fuchs, M. & Scheffler, M. Ab initio pseudopotentials for electronic structure calculations of poly-atomic systems using density-functional theory. *Comput. Phys. Commun.* **119**, 67–98 (1999).

[9] Monkhorst, H. J. & Pack, J. D. Special points for brillouin-zone integrations. *Phys. Rev. B* **13**, 5188 (1976).

[10] Romero, N. A. & Mattson, W. D. Density-functional calculation of the shock hugoniot for diamond. *Phys. Rev. B* **76**, 214113 (2007).

[11] Bradley, D. K. *et al.* Shock compressing diamond to a conducting fluid. *Phys. Rev. Lett.* **93**, 195506 (2004). URL `http://link.aps.org/doi/10.1103/PhysRevLett.93.195506`.